RSC Advances

PAPER

View Article Online
View Journal | View Issue

Cite this: *RSC Adv.*, 2018, **8**, 12190

In situ X-ray absorption spectroscopy study of $CuO–NiO/CeO_2–ZrO_2$ oxides: redox characterization and its effect in catalytic performance for partial oxidation of methane†

Lucía M. Toscani,[ab] M. Genoveva Zimicz,[c] Tereza S. Martins,[d] Diego G. Lamas[ef] and Susana A. Larrondo*[ab]

In this work we analyze the effect of adding CuO to a $NiO/Ce_{0.9}Zr_{0.1}O_2$ oxide by *in situ* X-ray absorption near-edge structure XANES technique in Ce L3, Ni K and Cu K absorption edges in terms of sample reducibility and catalytic activity. The oxidation states of Ce, Ni and Cu cations are followed up during temperature programmed reduction (TPR) experiments in diluted hydrogen and during catalytic tests for partial oxidation of methane (POM) reaction. Redox behavior was correlated to conventional fixed bed reactor results. The effect of firing temperature, crystallite size, $CeO_2–ZrO_2$ support and the presence of Cu and/or Ni as an active phase is also analyzed. Results showed a beneficial effect of CuO addition in terms of Ce and Ni reduction. A stronger interaction of NiO species with the support was revealed upon analysis of XANES reduction profiles in sample NiO/ZDC in contrast to bimetallic CuO–NiO/ZDC sample. Reduction onset temperature was found to depend on Ni crystallite size, being markedly promoted when samples exhibited low values of crystallite size both in supported and non-supported CuO–NiO species. *In situ* catalytic experiments for partial oxidation of methane showed a clear interplay between the redox behavior from the Ce in the $CeO_2–ZrO_2$ support and the Ni from the active phase. Sample NiO/ZDC exhibited a continuous reduction of Ce cations in $CH_4 : O_2$ feed flow, carbon formation was detected in X-ray Powder Diffraction (XPD) patterns and Ni re-oxidation was found to take place, clear indications of catalyst deactivation. In contrast, sample $CuO–NiO/Ce_{0.9}Zr_{0.1}O_2$ displayed a slight re-oxidation of Ce and no re-oxidation of Ni altogether with the suppression of carbon formation.

Received 19th February 2018
Accepted 23rd March 2018

DOI: 10.1039/c8ra01528g

rsc.li/rsc-advances

1. Introduction

Solid oxide fuel cells (SOFCs) stand as a promising technology to provide an efficient and clean energy supply. In the past few years much work has been conducted in order to lower the device operating temperature to the intermediate temperature (IT) regime (500–750 °C) to make this technology economically feasible.

In particular, the development of IT-SOFC anodes is centered in the fabrication of materials with high electronic and ionic conductivity to allow for hydrocarbons to be used as fuels.[1] These Mixed Ionic Electronic Conductors (MIECs) provide oxygen ions (O^{2-}) to the reaction sites enabling the oxidation of the fuel to take place all over the surface of the electrode. In addition, anode performance can be further enhanced developing materials with catalytic activity toward fuel decomposition into CO and H_2 mixtures that are easily electro-oxidizable into CO_2 and H_2O.[2]

$CeO_2–ZrO_2$ mixed oxides have been extensively studied due to their redox properties and oxygen storage capacity.[3,4] In this regard, the material with composition $Ce_{0.9}Zr_{0.1}O_2$ ('zirconia-doped ceria', ZDC) is active as a catalyst for total oxidation of methane (TOM) as well as a support for Ni-based catalysts for partial oxidation of methane (POM).[5–8] In fact, material NiO (60 wt%)/$Ce_{0.9}Zr_{0.1}O_2$ has been tested as an IT-SOFC anode,

[a]*UNIDEF, MINDEF, CONICET, Departamento de Investigaciones en Sólidos, CITEDEF, J. B. de La Salle 4397, 1603 Villa Martelli, Pcia. de Buenos Aires, Argentina. E-mail: slarrondo@citedef.gob.ar*

[b]*Instituto de Investigación e Ingeniería Ambiental, UNSAM, Campus Miguelete, 25 de Mayo y Francia, 1650 San Martín, Pcia. de Buenos Aires, Argentina*

[c]*Instituto de Física del Sur (IFISUR), Departamento de Física, Universidad Nacional del Sur (UNS), CONICET, Av. Alem 1253, 8000 Bahía Blanca, Pcia. de Buenos Aires, Argentina*

[d]*Universidade Federal de São Paulo – UNIFESP. Departamento de Química, Instituto de Ciências Ambientais, Químicas e Farmacêuticas, Rua São Nicolau 210, 2nd Floor, 09913-030, Diadema, São Paulo, Brazil*

[e]*CONICET/Escuela de Ciencia y Tecnología, UNSAM, Campus Miguelete, 25 de Mayo y Francia, 1650 San Martín, Pcia. de Buenos Aires, Argentina*

[f]*Departamento de Física de la Materia Condensada, Gerencia de Investigación y Aplicaciones, Centro Atómico Constituyentes, Comisión Nacional de Energía Atómica, Av. General Paz 1499, 1650 San Martín, Pcia. de Buenos Aires, Argentina*

† Electronic supplementary information (ESI) available. See DOI: 10.1039/c8ra01528g

exhibiting an excellent performance due to the presence of cerium in its structure which contributed to the electrode enhanced reducibility and ionic conductivity due to the partial reduction of cerium cation.[9,10] Nonetheless, in reducing atmospheres and due the elevated Ni content required to ensure electrical percolation, carbon formation is favored when hydrocarbons are used as fuels. Coke deposition takes place at adjacent Ni sites, which promote the nucleation and growth of carbon filaments blocking the active sites for fuel activation and, eventually, leading to the fracture of the device.[8,11] In this sense, Zimicz *et al.* studied, in sample 60 wt% NiO/40 wt% $Ce_{0.9}Zr_{0.1}O_2$, the evolution of the crystal structure with temperature and operating conditions and monitored the oxidation states of Ce and Ni by *in situ* X-ray absorption near-edge structure (XANES) and X-ray powder diffraction XPD experiments in reducing atmospheres.[8] They reported a complete Ni reduction at temperatures above 650 °C and total conversion of methane to syngas at temperatures higher than 700 °C. Ni was confirmed to be the active center for POM and the ratio of Ce^{4+}/Ce^{3+} was found to be responsible to deliver oxygen from the lattice to produce CO_x species. Nonetheless, experiments confirmed the formation of carbon filaments due to the large amount of NiO in the sample.

As a strategy to reduce carbon deposition, Ni-based bimetallic catalysts had been widely studied for hydrocarbon oxidation and reforming reactions.[1,12] In particular, Cu–Ni catalysts stand as a promising alternative as they have shown enhanced reducibility and increased coke resistance due to the addition of Cu which is not active for CH_4 decomposition.[13–15]

Cu active phase has been deposited over the traditional Ni/yttria-stabilized zirconia (YSZ) anodes suitable for high-temperature SOFC operation, and carbon formation during direct hydrocarbon utilization was considerably suppressed in Cu-containing materials.[13] Afterward, in light of lowering anode operating temperature, CeO_2-based supports have been tested in intermediate temperature SOFC conditions altogether with different ratios of Cu : Ni in the active phase.[16,17] In particular, Hornés *et al.* studied the effect of partially substituting Ni by Cu in Ni/CeO_2 and Ni/$Ce_{0.9}Gd_{0.1}O_{2-x}$ anodes in redox, catalytic and electro-catalytic performance.[18] The authors performed *in situ* X-ray absorption spectroscopy (XAS) studies with CH_4 as a fuel and reported a beneficial effect in the reduction of carbon deposits in Cu-containing samples and a promoting effect of the Gd present in the support in terms of the enhancement of oxygen transport properties in the material that led to an improved CH_4 oxidation.

In the past few years, several studies have been conducted in order to understand the redox behavior of all Cu, Ni and Ce cations present in operating conditions, especially for catalytic applications where low metallic loadings and low calcination temperatures are sufficient to guarantee reactant conversion.[13–20] Matte *et al.* studied 20 wt% Cu and 20 wt% Ni/CeO_2 nanoparticles in reducing atmospheres by means of XAS and transmission electron microscopy (TEM) techniques and reported a strong interaction between Ni and CeO_2 which enhanced Ni reducibility in diluted H_2 feed flows.[19] De Rogatis *et al.* studied 5 wt% Cu-5 wt% Ni/Al_2O_3 for POM applications and reported a beneficial effect of Cu addition to the system in terms of lowering the onset temperature for POM reaction and negligible carbon formation.[15]

Song *et al.* studied anodes with Cu, CuNi and Ni supported over $Ce_{0.9}Zr_{0.1}O_2$ and over CeO_2 and reported an improved electrochemical performance of CeO_2–ZrO_2 support when compared to CeO_2 support in terms of thermal stability and anode activity.[10] Furthermore, the bimetallic sample (40 wt% CuNi/ZDC) exhibited a superior electrochemical performance when compared to the monometallic one. However, no redox or catalytic tests were performed to analyze the effect of the species present in the anode in its effect in the electrode performance. In this sense, in a previous work, the authors studied the effect of the partial replacement of NiO for CuO in NiO (60 wt%)/$Ce_{0.9}Zr_{0.1}O_2$ cermet in catalytic activity for POM and redox behavior in conventional laboratory tests showing the beneficial effect of Cu addition in the suppression of carbon formation and lowering of anode resistance in the bimetallic sample.[14] However no detailed *in situ* studies have been performed to analyze the redox state of Ni, Cu and Ce and their effect on catalytic activity.

Therefore, the aim of this work is to study in detail, by means of *in situ* XANES spectroscopy experiments in dispersive mode, the oxidation state of the cations present both in the support and in the metallic phases in NiO/ZDC and CuO–NiO/ZDC cermets under diluted hydrogen and CH_4/O_2 atmospheres in order to correlate redox properties with catalytic activity. The effect of support and firing temperature is also discussed.

2. Experimental

2.1 Sample preparation

The $Ce_{0.9}Zr_{0.1}O_2$ (ZDC) support was synthesized by the glycine/nitrate combustion process previously reported elsewhere and calcined at 600 °C for 2 h in order to eliminate carbonaceous residues.[21] Impregnation of CuO and/or NiO was carried out through the incipient wetness technique from the corresponding nitrates dissolved in ethanol solutions. The resulting material was calcined for 2 h at 1000 °C. The following samples were prepared: ZDC: [$Ce_{0.9}Zr_{0.1}O_2$]; NiO/ZDC: [NiO (60 wt%)/ZDC]; CuO–NiO/ZDC: [CuO (30 wt%)–NiO (30 wt%)/ZDC]; CuO/ZDC: [CuO (60 wt%)/ZDC]. In addition, in order to assess the effect of firing temperature and support, two samples were prepared using the glycine/nitrate synthesis procedure and fired at 350 °C for 2 h: CuO–NiO/ZDC (T_c = 350 °C) and non-supported CuO–NiO (T_c = 350 °C).

2.2 Catalyst characterization

Sample surface area was evaluated using N_2 physisorption at nitrogen normal boiling temperature (−196 °C) with a Quantachrome Corporation Autosorb-1 equipment. Samples were previously degassed with He at 50 °C for 24 h Results were obtained following the five point Brunauer–Emmett–Teller (BET) method.

Solid structure was studied with XPD technique, using a Phillips PW3710 diffractometer operated with Cu-Kα radiation

and a graphite monochromator. Data was collected in the angular region of $2\theta = 20$–$80°$ with a step size of 0.03° and a time per step of 4 s. The average crystallite size was calculated by means of the Scherrer equation using the (111) reflection for the fluorite structure and the (111) and (101) reflections for the CuO and NiO phases respectively.

Sample morphology was studied by means of scanning electron microscopy (SEM) technique using a Zeiss Electron Beam SEM-Supra 40. The powdered samples were deposited over an adhesive carbon-filled conductive tape to avoid charging problems.

2.3 Conventional laboratory TPR and catalytic activity tests

Temperature programmed reduction (TPR) experiments were performed in a Micromeritics Chemisorb 2720 equipment in order to assess sample reducibility. The equipment determines the H_2 uptake with a Thermal Conductivity Detector (TCD) previously calibrated. Tests were carried out from room temperature up to out 800 °C, following a heating ramp of 10 °C min^{-1} in a flow consisting of 5 mol% H_2 in Ar (50 cm^3 (STP) min^{-1}). Prior to each measurement, samples were pre-treated in pure He flow during 1 h at 300 °C with heating and cooling rates of 10 °C min^{-1} in order to eliminate any adsorbed species in the solid surface.

Conventional catalytic activity tests for partial oxidation of methane were performed in a quartz fixed bed reactor operated at atmospheric pressure in the temperature range: 500–750 °C. Reactor inlet feed consisted in a mixture of 3.1 mol% CH_4, 1.2 mol% O_2 with N_2 balance; with a total feed flow of 436 cm^3 min^{-1}. These TPR and catalytic activity test results were previously reported but are included in the present work in order to compare and complement *in situ* TPR and catalytic activity experiments.[14]

2.4 *In situ* XANES experiments

In situ XANES studies were performed in the Ce L3, Ni K and Cu K absorption edges of the D06A-DXAS dispersive beamline from the Brazilian Synchrotron Light Laboratory (LNLS), Campinas, Brazil (proposal: XAFS1-15329). A Si (111) monochromator was used altogether with a CCD detector to collect the absorption spectrum in transmission mode. Self-supporting discs were prepared by mixing the sample powder with boron nitride that has no significant absorption in the energy ranges used. The catalyst mass in the discs was calculated in order to obtain a total absorption ratio of 1.5. In the experiments 12 mg of powder sample and 73 mg of boron nitride were used. Sample discs were located in a sample-holder with a thermocouple attached to it. The sample holder was placed in a quartz reactor, with inlet and outlet gas lines, and located in a furnace with temperature control. Inlet gas composition was set with a gas-mixing station provided with mass flow controllers and exit composition was assessed with a Pfeiffer Omnistar mass spectrometer.

In situ TPR experiments were carried out by heating the sample in a 5 mol% H_2 (He balance) flow with a heating rate of 10 °C min^{-1} up to 800 °C following the same procedure used in conventional laboratory TPR experiments.

In situ catalytic tests were performed to assess sample activity towards partial oxidation of methane using a reactor inlet flow consisting of a mixture of: 1.3 cm^3 min^{-1} O_2, 3.4 cm^3 min^{-1} CH_4 and 104.3 cm^3 min^{-1} He. Molar feed ratio ($CH_4 : O_2 = 2.6$) was superior to the stoichiometric one for POM ($CH_4 : O_2 = 2$) in order to work in a methane excess atmosphere, a prevailing condition in a SOFC anode. The spatial time used was of $\tau =$ 0.11 mg catalyst min cm^{-3}. Measurements were performed in the temperature range: 500–750 °C, and a dwell time at each temperature of 30 min, following a heating ramp of 10 °C min^{-1}. All catalytic tests were carried out emulating conventional laboratory experiments in order to further analyze the performance of the samples.

Data analysis was performed by means of the Athena software included in the IFEFFIT software package.[22] A linear combination fitting of standard spectra was carried out in order to assess the fractions of reduced and oxidized species in the samples during the course of the experiments. Before proceeding with the linear combination fitting, background subtraction and spectrum normalization was carried out. For the data obtained in the Ce L3-edge, the fitting was performed using a $Ce(NO_3)_3 \cdot 6H_2O$ disc as a Ce(III) standard and the initial spectrum of each sample as a Ce(IV) standard. By following this procedure, the degree of reduction of the samples is obtained and not the absolute Ce(III) content. In the case of Cu K and Ni K-edge experiments, Cu_2O, CuO and NiO powders were used as a reference of Cu(I), Cu(II) and Ni(II) species respectively. To assess the amount of Ni^0 and Cu^0, the spectra corresponding to a Ni and a Cu foil were used as standards respectively. However, the fitting was also carried out using as standards of the reduced samples the last spectra recorded at 800 °C in H_2 flow. The fitting results obtained by both procedures exhibited less than 5% error in the whole temperature range but the fitting was qualitatively improved. It should be noticed that Ni and Cu foils were recorded at 25 °C and reduced spectra were recorded at temperatures over 400 °C. High temperatures tend to diminish the intensity of oscillations in the absorption profile due to higher thermal disorder thus leading to slight differences between the standard spectra and reduced sample spectra.[23]

3. Results and discussion

3.1 Characterization of the catalysts

XPD patterns of fresh samples corresponding to the support (ZDC) and impregnated samples (CuO/ZDC, NiO/ZDC and CuO–NiO/ZDC) are presented in Fig. 1. In all cases the phase corresponding to the fluorite-type structure (space group $Fm\bar{3}m$) of ceria can be identified as well as the oxide phases in supported samples (CuO in CuO/ZDC, NiO in NiO/ZDC; CuO and NiO in CuO–NiO/ZDC). In Table 1 the average crystallite size (D_{XPD}) of ZDC, CuO and NiO phases are presented altogether with the BET specific surface area (S_{BET}) of each sample. The results show there is an increase in the crystallite size of the ZDC phase after impregnation and firing at 1000 °C. In addition, the

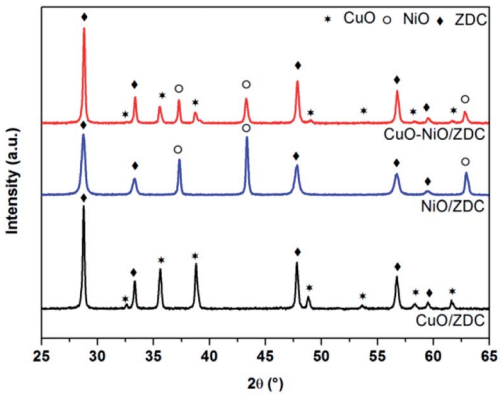

Fig. 1 XPD patterns of fresh samples calcined at 1000 °C.

crystallite sizes of ZDC and NiO increase with CuO loading, indicating that the presence of CuO enhances the sintering of both NiO and the ZDC support. On the other hand, textural characterization results show a significant decrease in S_{BET} when samples are fired at 1000 °C and a minor drop with increasing CuO loading.

3.2 *In situ* XANES experiments

3.2.1 Ce L3-edge. In Fig. 2 Ce(IV) and Ce(III) reference spectra are plotted altogether with the last spectrum recorded for sample CuO/ZDC at 800 °C in 5 mol% H_2/He atmosphere Ce(IV) spectrum corresponds to the initial profile recorded in ambient temperature. This spectrum exhibits two peaks near the absorption edge which correspond to characteristic electronic transitions of Ce^{4+} compound ($2p_{3/2} \rightarrow (4f^1L)5d^1$ and $2p_{3/2} \rightarrow (4f^0)5d^1$, respectively).[4] In the case of Ce(III) spectrum, a $Ce(NO_3)_3 \cdot 6H_2O$ sample was used as a reference, which exhibits a single peak characteristic of Ce^{3+} $2p_{3/2} \rightarrow (4f^1)5d$ transition. These reference spectra can be used as a fingerprint of each oxidation state. Therefore, in order to obtain the degree of reduction of a sample with an unknown Ce^{4+}/Ce^{3+} content, a linear combination fit of both spectra was performed as detailed in the experimental section. In the inset of Fig. 2 the result of the linear combination fitting is depicted, exhibiting a very good agreement with the experimental data in the XANES energy range considered (absorption edge ± 20 eV). In all samples studied, the maximum error in the Ce^{3+} and Ce^{4+} fractions registered after fitting procedure was of 0.5%.

In Fig. 3 a selection of XANES profiles of samples ZDC, CuO/ZDC, NiO/ZDC and CuO–NiO/ZDC are plotted against temperature. These spectra were obtained during *in situ* experiments in 5 mol% H_2/He atmosphere upon heating up to 800 °C. It is clear, in the last spectra recorded at 800 °C, that the Ce(III) peak contribution is greater for NiO/ZDC, CuO–NiO/ZDC and CuO/ZDC samples compared to sample ZDC.

In Fig. 4 the degree of reduction of the three samples is plotted as a function of temperature. In all cases the degree of reduction rises with increasing temperatures. The reduction onset temperature was similar for all three samples at about 200 °C with no significant differences in their redox behavior in the temperature range: 25–650 °C. On the contrary, in the range 650–800 °C, sample ZDC exhibited the lowest degree of reduction (α_{Ce}) with a final value of 27%. In the case of NiO and CuO–NiO loaded samples, the final degree of reduction was of 41% for both samples and of 43% for the CuO-loaded sample at 800 °C. It is noteworthy that CuO/ZDC and CuO–NiO/ZDC samples presented higher reduction values in the whole temperature range, evidencing enhanced reduction kinetics for Cu-containing samples when compared to the NiO/ZDC sample.

In the inset of Fig. 4 a simulation of the TPR profiles is presented. This simulation was performed by fitting the reduction profiles presented in Fig. 4. Details from the fitting of reduction profiles and building of element specific TPR profiles are included in the ESI† section. A set of sigmoidal curves was used to adjust the data points and the resulting curve was then differentiated to obtain the TPR profile as a function of temperature. This method allows a straightforward comparison with most reported results regarding CeO_2 reduction profiles performed with conventional TPR experiments with a TCD detector. Fitting was performed assuming that the Ce reduction takes place in two steps: the first step is generally attributed to

Table 1 Structural and morphological characterization

Sample	S_{BET} ($m^2\ g^{-1}$)	D_{XPD} ZDC (nm)	D_{XPD} NiO (nm)	D_{XPD} CuO (nm)
ZDC (T_c = 600 °C)	45	9	—	—
NiO/ZDC (T_c = 1000 °C)	8	25	61	—
CuO–NiO/ZDC (T_c = 1000 °C)	5	55	75	41
CuO/ZDC (T_c = 1000 °C)	3	57	—	45
CuO–NiO/ZDC (T_c = 350 °C)	19	10	20	49

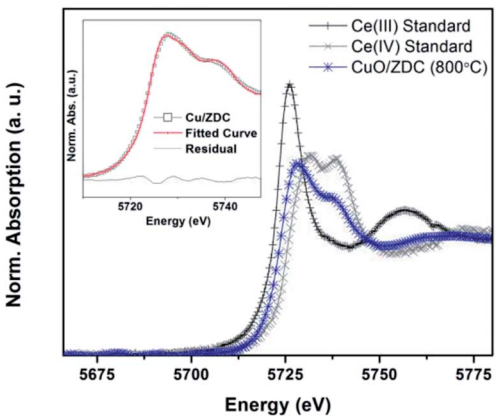

Fig. 2 XANES Ce(III) and Ce(IV) reference spectra plotted altogether with the last spectra recorded at 800 °C in 5 mol% H_2/He during *in situ* TPR experiment of CuO/ZDC sample. In the inset the experimental data points (squares) and the fitted profile (solid line) are plotted in the energy range in which the fittings were performed.

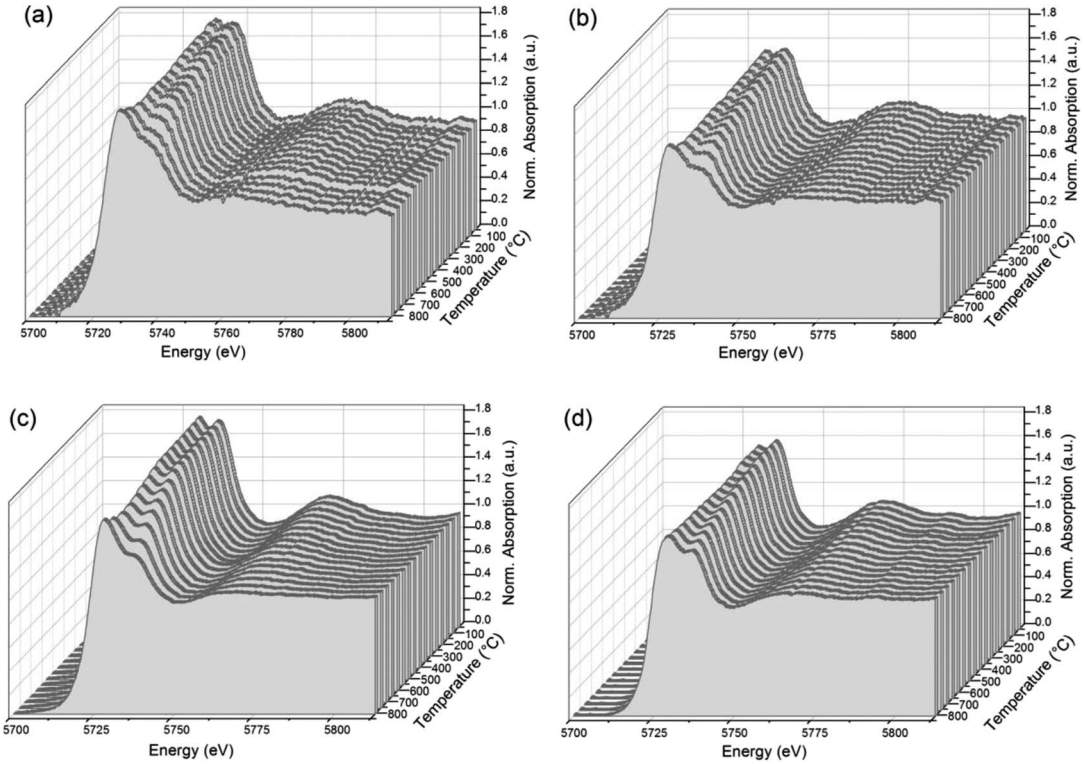

Fig. 3 *In situ* XANES profiles collected upon heating in 5 mol% H_2/He for samples: (a) CuO–NiO/ZDC, (b) NiO/ZDC, (c) CuO/ZDC, and (d) ZDC.

the reduction of less coordinated surface species, whilst the high temperature step is usually associated to bulk reduction.[24] The simulated TPR profiles are consistent with this assumption and exhibit two well defined peaks. In this case, the low temperature peak maximum was estimated at 589 °C, 439 °C, 431 °C and 416 °C for ZDC, NiO/ZDC, CuO/ZDC and CuO–NiO/ZDC respectively. This is an indication that the addition of NiO and/or CuO to the ZDC system shifts the reduction profile of ZDC toward lower temperatures. However, this effect is even more pronounced for the CuO-containing samples compared to the NiO/ZDC sample. This can be supported by the fact that the high temperature peak is also shifted toward lower temperatures when CuO is added to the system, being 712 °C and 761 °C the corresponding peak maxima temperatures for samples CuO/ZDC and CuO–NiO/ZDC respectively. It is worth noticing that in the temperature range analyzed the high temperature peak is not resolved neither for ZDC nor NiO/ZDC.

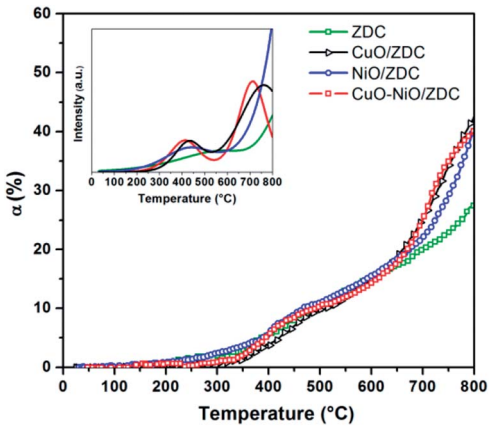

Fig. 4 Degree of Ce reduction [$\alpha = Ce^{3+}/(Ce^{4+} + Ce^{3+})$] obtained for ZDC, CuO/ZDC, NiO/ZDC and CuO–NiO/ZDC samples during the course of the TPR experiment. In the inset: simulated Ce-TPR profiles obtained from fitting the profiles with two step functions and subsequent differentiation.

The enhancement in ceria reducibility has been reported in ceria-based supports combined with catalytically active metals and transition metals, in particular with Cu and Ni.[25–27] The mechanism proposed to explain this effect is the dissociative adsorption of hydrogen on the surface of the metallic phase followed by hydrogen spillover onto the oxide support, enabling the reduction of Ce^{4+} at lower temperatures in contrast to the bare support.[28] In particular, in the case of Ni supported on ceria-based supports, Sharma *et al.* observed by means of electron microscopy a preferential reduction of ceria in the surroundings of Ni particles evidencing the occurrence of hydrogen spillover from Ni to the oxide support.[28] In the case of Cu–CeO_2 systems, it has been proposed that H_2 spills over highly dispersed copper species to promote the concomitant reduction of both CuO and CeO_2 support.[27,29] In line with this, the fact that ceria is more easily reduced in CuO–NiO/ZDC sample when compared to CuO/ZDC at low temperatures (T < 600 °C) can be related to the metallic loading in both samples since their BET specific surface areas are similar. The bimetallic sample contains only 30 wt% CuO whereas the monometallic sample contains 60 wt% CuO. This higher oxide content led to

a more agglomerated sample since CuO has a high tendency toward sintering due to a low melting point compared to NiO.[30] This agglomeration is visible in the sample crystallite sizes (41 and 45 nm for CuO–NiO/ZDC and CuO/ZDC respectively), in BET specific surface area values (5 $m^2 g^{-1}$ and 3 $m^2 g^{-1}$ for CuO–NiO/ZDC and CuO/ZDC respectively) and in SEM images presented in Fig. 5 where sample agglomeration is evident with increasing CuO content. This agglomeration can affect spillover mechanism as H_2 is expected to spill over highly dispersed copper species, being most favored in the less agglomerated bimetallic sample when compared to the monometallic one.

3.2.2 Ni K-edge. In Fig. 6 the degree of Ni reduction is presented as a function of temperature. In it, up to 560 °C, CuO–NiO/ZDC sample exhibited the highest values of nickel reduction and an onset temperature of 345 °C, which was 40 °C lower than for the NiO/ZDC sample. Between 560 °C and 630 °C, NiO/ZDC presented slightly higher reduction values (<5% difference). Above 630 °C both samples were completely reduced. TPR profile simulations are presented in the inset of Fig. 6, where the two characteristic NiO reduction peaks can be observed. The low temperature peak is usually ascribed to the reduction of relatively free nickel surface species, whereas the high temperature peak is generally attributed to NiO strongly interacting with the support.[31] It is worth noticing that Cu addition to the Ni sample not only moved the reduction profile to lower temperatures but also diminished the area under the high temperature peak, implying that there are fewer species that strongly interact with the support.

The $Cu^{2+} \rightarrow Cu^0$ (+0.34 V) reduction reaction has a lower reduction potential compared to the $Ni^{2+} \rightarrow Ni^0$ reaction (−0.26 V), which allows for the former reaction to take place at lower temperatures.[32] As described in the previous section, one of the proposed mechanisms for bimetallic Cu–Ni samples supported on ceria-based materials includes a dissociative adsorption of H_2 over the surface of highly dispersed Cu species followed by H_2 spillover which triggers the concomitant reduction of CuO, NiO and CeO_2. This can explain why Ni reduction in the bimetallic CuO–NiO/ZDC sample is markedly enhanced, especially in the lower temperature range (300–550 °C) when compared to the monometallic NiO/ZDC sample. It is interesting to point out that this enhancement in the sample reducibility was not a result of a crystallite size effect since sample CuO–NiO/ZDC exhibited a Ni particle size of 75 nm compared to the 61 nm of Ni crystallites in sample NiO/ZDC.

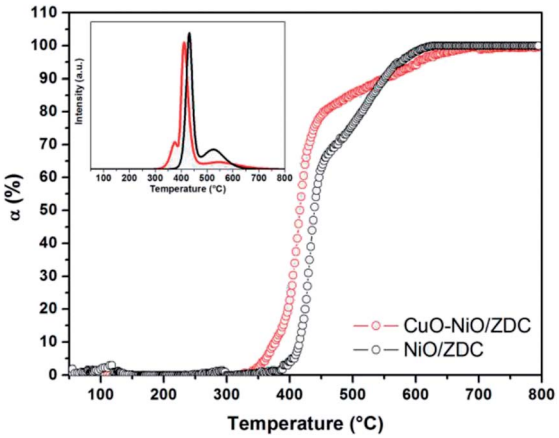

Fig. 6 Degree of Ni reduction [$\alpha = Ni^{2+}/(Ni^{2+} + Ni^0)$] obtained for the CuO–NiO/ZDC and NiO/ZDC samples during the course of the TPR experiment. In the inset: simulated Ni-TPR profiles.

Finally, a difference in the initial stage of both reduction profiles can be acknowledged: NiO/ZDC sample exhibited virtually no lag phase whereas sample CuO–NiO/ZDC evidenced a pronounced induction phase. This feature resulted in a small peak in the simulated Ni-TPR profile, visible in Fig. 6. Further analysis on this feature will be addressed in the following section were the effect of support and firing temperature are discussed.

3.2.2.1 Effect of support and firing temperature on Ni reduction. XPD patterns of CuO–NiO/ZDC samples fired at 350 °C and 1000 °C are presented in Fig. 7 and morphological and structural data is presented in Table 1. These results show there is an increase in the crystallite sizes of both ZDC and NiO phases when CuO–NiO/ZDC is fired at 1000 °C, whilst the CuO crystallite size remains significantly unchanged in both samples.

In order to analyze the effect of the ceria support on Ni reduction, a non-supported CuO–NiO sample prepared by the same glycine-nitrate route was synthesized and fired at 350 °C. The results from XANES TPR experiments performed with the three CuO–NiO samples, the two supported and the non-supported one, are presented in Fig. 8 where the degree of Ni reduction (α_{Ni}) is plotted against temperature. The reduction onset temperature is lowest for the non-supported sample and increases with firing temperature. Moreover, the kinetics of the initial stage of the reduction is visibly different: in the case of the CuO–NiO sample, the beginning of the reduction is quite

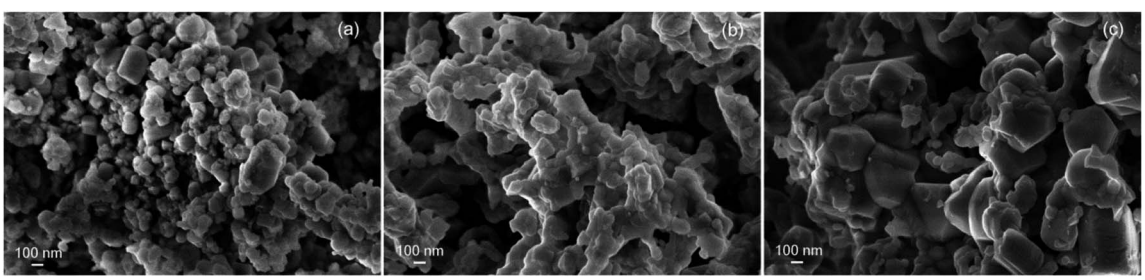

Fig. 5 SEM images of fresh samples fired at 1000 °C (a) NiO/ZDC, (b) CuO–NiO/ZDC, (c) CuO/ZDC.

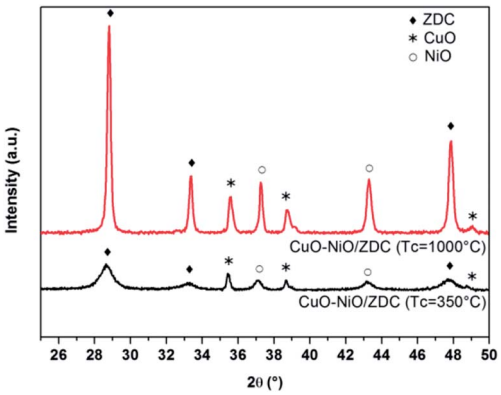

Fig. 7 XPD patterns of fresh sample CuO–NiO/ZDC fired at 350 °C and 1000 °C.

abrupt, whilst for the supported sample fired at 350 °C there is a slight lag. This delay is even more pronounced for the sample fired at 1000 °C, evidenced with a small slope up to $\alpha = 20\%$.

In all cases the reduction takes place in more than one step. This is an indication that there are different Ni species present in the samples, each with different redox capabilities. In the case of the CuO–NiO sample, even though there is no support, the interaction of Cu and Ni particles influence the reduction mechanism of Ni particles. Although Ni^0 and Cu^0 are completely miscible in each other, potentially allowing for uniform alloying to take place in reducing atmospheres, CuO reduction is thermodynamically favored when compared to NiO reduction.[30] Li *et al.* studied Ni–Cu samples supported on TiO_2 and reported that, although in most of the samples uniform alloying is obtained, a Ni or Cu surface enriched alloy can be formed, depending mainly on Cu reduction kinetics, which was found to markedly enhance Ni reduction.[33] In our results, after TPR experiments, a Ni-rich alloy is formed altogether with non-alloyed Cu for CuO–NiO/ZDC sample as shown in Fig. 9, where XPD patterns of samples after TPR experiments are plotted. On the other hand, another reason that might account for a two-step reduction in the CuO–NiO sample might be the broad particle size distribution, affecting H_2 diffusion with the concomitant delay in Ni^{2+} reduction.

Evidence presented in the literature is ambiguous regarding to the effect of CeO_2-based supports on Ni reduction. A strong metal support interaction (SMSI) is frequently called upon to explain the different reduction profiles obtained.[34] Both an electronic and a geometric factor effect of this SMSI have been reported to affect the reduction kinetics of Ni particles supported on ceria supports.[19,35] The former involves an electronic charge transfer between the Ni nanoparticle and the support, whilst the latter implies the migration of Ce reduced species to the surface of the metallic nanoparticle thus modifying its catalytic properties.[35] The electronic effect has been found to promote the reduction of CeO_2-supported nanoparticles, whereas the geometric factor is detrimental for Ni reduction as a consequence of the physical blockage of active sites.

Matte *et al.* studied the effect of CeO_2 support on Ni nanoparticles reduction. They studied Ni/CeO_2 and non-supported Ni samples.[19] In their work 20 wt% Ni was supported over CeO_2 and no calcination stage was performed prior to reduction treatment, which led to a mean Ni crystallite size of 3.5 nm. They reported an enhanced reduction kinetics for Ni/CeO_2 sample compared to the Ni nanoparticles after a mild reduction treatment in 5 mol% H_2/He up to 500 °C. After the reduction treatment the authors found evidence of the geometrical SMSI effect on TEM images that evidenced the migration of Ce species over the Ni nanoparticles. However, they ascribe the enhanced reducibility of the supported samples to the electronic effect which is expected to facilitate reduction by charge transfer at low temperatures.

In our case, the opposite was found since the non-supported NiO particles were reduced at significantly lower temperatures in CuO–NiO than in CuO–NiO/ZDC sample. It is highly likely that the reason for this different behavior lies in the crystallite size. The three samples hereby compared presented different Ni crystallite sizes: <7 nm, 20 nm and 75 nm for samples CuO–NiO (T_c = 350 °C), CuO–NiO/ZDC (T_c = 350 °C) and CuO–NiO/ZDC (T_c = 1000 °C) respectively. It is therefore noteworthy that sample CuO–NiO with the lowest onset temperature for the reduction of Ni presented the smallest crystallite size. In this

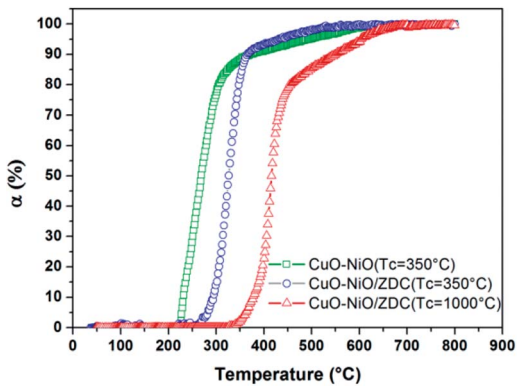

Fig. 8 Degree of Ni reduction [$\alpha = Ni^0/(Ni^{2+} + Ni^0)$] obtained for samples: CuO–NiO/ZDC fired at 350 °C and at 1000 °C and CuO–NiO (non-supported) fired at 350 °C during the course of TPR experiments.

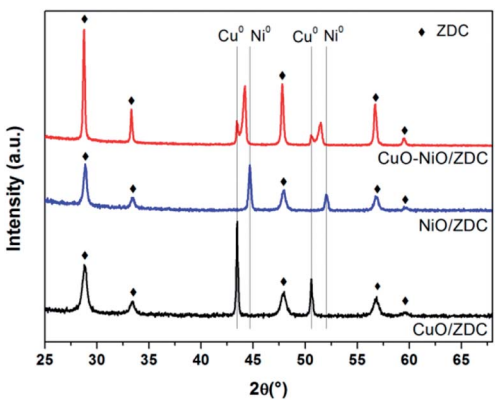

Fig. 9 XPD patterns of samples fired at 1000 °C after conventional laboratory TPR experiments.

sense, the reduction profile of sample CuO–NiO/ZDC ($T_c = 1000$ °C) was shifted towards higher temperatures. Matte *et al.* tested samples with very small crystallite sizes that enabled a reduction at low temperatures (<200 °C) thus enabling the electronic effect to prevail at low temperatures, whilst the supported samples hereby tested exhibited Ni crystallite sizes larger than 20 nm.[19]

In Fig. 10 SEM images of fresh samples of CuO–NiO (T_c = 350 °C) and CuO–NiO/ZDC (T_c = 350 °C) are presented. Both samples present clear morphological differences. The non-supported sample is densely agglomerated whilst the supported sample exhibits a homogeneous morphology, an enhanced particle dispersion and high porosity. Therefore, it is clear that the addition of CeO_2–ZrO_2 to the system contributes to obtain a material with an improved texture and morphology. Nonetheless this is not enough to promote the reduction at lower temperatures than the ones achieved by the non-supported sample. Then, it is plausible that in addition to the crystallite size effect, the interaction of Ni particles with the CeO_2–ZrO_2 support can contribute to a delayed reduction kinetics.

Finally, comparing results from sample CuO–NiO/ZDC fired at different temperatures, there is a visible shift in the Ni reduction profile towards lower temperatures for sample calcined at 350 °C when compared to sample calcined at 1000 °C. The first reduction step, which is usually ascribed to the reduction of surface species, as described in the previous section, is steeper and reaches a higher degree of reduction for CuO–NiO/ZDC (T_c = 350 °C) compared to sample CuO–NiO/ZDC (T_c = 1000 °C). This might be related to both textural and morphological features. First, sample CuO–NiO/ZDC (T_c = 350 °C) exhibited a larger BET specific surface area value (19 m^2 g^{-1}) compared to the value measured for sample CuO–NiO/ZDC (T_c = 1000 °C) (5 m^2 g^{-1}). This improved texture leads both to a more porous structure, triggering a more efficient H_2 diffusion through the sample and also to a larger amount of gas-accessible Ni sites to facilitate the reduction process. In addition to this, a noteworthy difference between the two reduction profiles is the extent of the second reduction step, usually attributed to the reduction of bulk species or species strongly bound to the support. In the sample fired at low temperature the second reduction step is quite small, whilst for the sample fired at high temperature this step is considerable. This might be ascribed to a large aggregation of NiO species that are less prone to be reduced. The mean NiO crystallite size for the sample calcined at 1000 °C was of 75 nm whereas for sample calcined at 350 °C this value was of 22 nm. Therefore a larger crystallite size and a broader particle size distribution for sample CuO–NiO/ZDC (T_c = 1000 °C) could explain the differences in the extent of the second step. Not to mention the fact that the treatment at higher temperatures can sharpen the interaction between NiO and the support contributing to a slower reduction kinetics.

3.2.3 Cu K-edge. In Fig. 11 the *in situ* XANES spectra recorded during the TPR experiment of the bimetallic CuO–NiO/ZDC sample in the Cu K-edge are presented. These spectra were recorded from ambient temperature up to 800 °C with a 10 °C min^{-1} temperature ramp as described in the Experimental section. The absence of isosbestic points in this plot is an indication of the presence of an intermediate phase during the reduction procedure.[36] In this case, Cu^{2+} is first reduced to Cu^{+} to be further reduced to Cu^{0}. In Fig. 12a the linear combination fitting results are presented for the CuO–NiO/ZDC in the Cu K-edge. In it, a small peak with its maxima at 388 °C is exhibited which corresponds to the Cu^{+} formation and

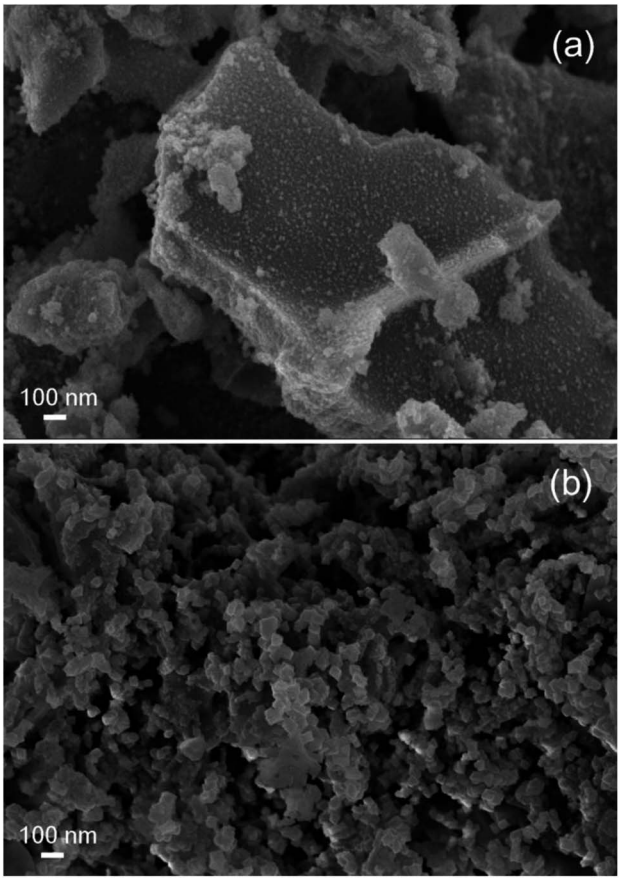

Fig. 10 SEM images of (a) sample CuO–NiO (non-supported) fired at 350 °C and (b) sample CuO–NiO/ZDC fired at 350 °C.

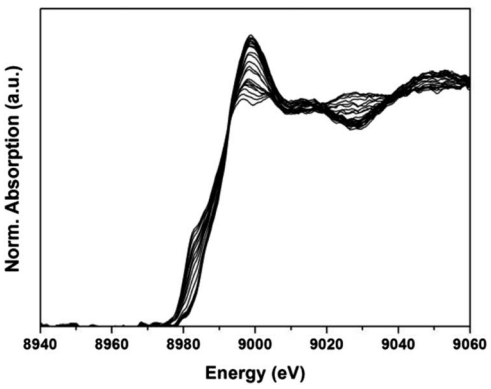

Fig. 11 XANES normalized absorption profiles of sample CuO–NiO/ZDC recorded during the *in situ* TPR experiments in the Cu K-edge.

subsequent reduction. The fact that an intermediate Cu_2O phase is formed depends on reduction conditions such as feed composition and temperature ramping.[37] In this case, a mild reduction was carried out since feed composition was of 5 mol% H_2/He and the temperature ramp was of 10 °C min^{-1}, indicating that these set of conditions were adequate to prompt a Cu^+ mediated reduction. Although no traces of Cu_2O were detected after TPR experiments by means of XPD, as shown in Fig. 9, in samples subjected to a reducing atmosphere during POM catalytic experiments, the XPD profiles recorded after catalytic tests which will be presented in the following sections showed that samples were partially reduced, with peaks corresponding to Cu, Cu_2O, Ni and CuNi alloy phases.

Finally, in Fig. 12b the simulated reduction profile of copper species is presented for the bimetallic sample. An asymmetric peak is observed which can be deconvoluted into two peaks. The first is usually ascribed to the reduction of highly dispersed copper species, while the second one to bulk CuO.[38] It is worth noticing that these highly-dispersed species are thought to be responsible for enhancing both CuO, NiO and CeO_2 reducibility in the CuO–NiO/ZDC cermet.[27]

3.3 Conventional laboratory TPR *vs. in situ* XANES TPR

In Fig. 13a the simulated TPR profiles for CuO–NiO/ZDC and NiO/ZDC samples are presented. Reduction contributions from Cu K, Ni K and Ce L3-edges are included. All contributions were added up taking into account the amount of hydrogen consumed from the stoichiometry of each reduction reaction. Results were normalized per mole of Ce for comparison purposes. These results can be compared to the conventional laboratory TPR experiments presented in Fig. 13b. In the case of the CuO–NiO/ZDC sample both XANES and laboratory TPR profiles present an unresolved curve with two peaks that correspond to Cu and Ni reduction. The Ni : Cu peak intensity ratio is very similar 1.2 and 1.1 for the laboratory and *in situ* experiments respectively. However, the laboratory TPR presents a broader profile with a lower onset reduction temperature and a small shoulder in the first peak at 200 °C. Sensitivity of reduction profiles as to peak shape, maximum temperature and

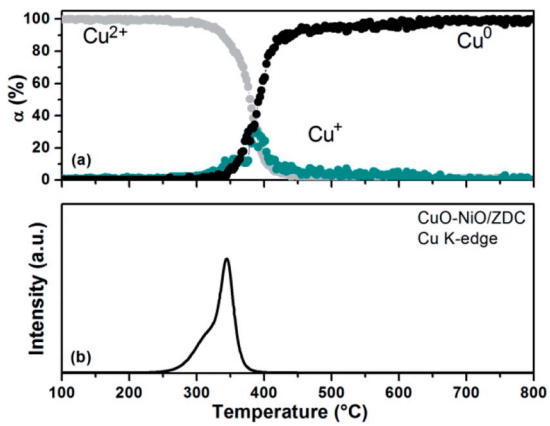

Fig. 12 (a) Degree of Cu^{2+} and Cu^+ reduction of sample CuO–NiO/ZDC against temperature during the TPR experiment in the Cu K-edge. (b) Simulated TPR profile as a function of temperature.

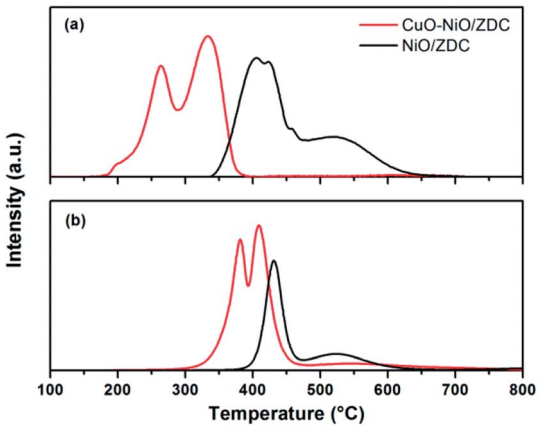

Fig. 13 (a) Conventional laboratory TPR profiles using a TCD detector (b) simulated TPR profiles from XANES experiments.

curve resolution in conventional TPR experiments using a thermal conductivity (TCD) detector are deeply influenced by the selection of experimental conditions.[25,39] Therefore, differences in experimental setup can lead to different TPR profiles. Temperature ramping, hydrogen concentration and total feed flow were kept the same for both experiments, nonetheless it should be noted that in the conventional laboratory experiments the amount of catalyst sample (167 μmol) was chosen in order to guarantee that no hydrogen exhaustion from the feed took place at peak maximum. Care was taken as well to obtain a good noise-to-signal ratio following standard parameter selection.[39] In the case of the *in situ* XANES tests, 122 μmol of sample were used diluted in 0.07 g of boron nitride in order to ensure that no excessive energy absorption took place. The fact that the mass of sample was higher and that the bed remained undiluted in the former case could lead to both mass and heat transfer limitations in the course of the TPR procedure. The increment of mass sample has proven to diminish peak resolution and provoke hydrogen concentration and temperature gradients in the sample bed.[39] This could also explain differences in peak shape for NiO/ZDC in both experiments. Two peaks can be clearly identified in both experiments. However, in the case of the conventional test, peaks are less separated and small shoulders can be observed in the low temperature peak. Furthermore, this difference in mass sample led to a larger spatial time ($\tau = m_{catalyst}$/total feed flow) for the laboratory test experiments which could explain the lower onset temperature obtained in these profiles. Therefore, the above results point out the importance of the *in situ* XANES experiments to distinguish the different features present in TPR profiles and to obtain an accurate quantification of the extent of sample reduction, especially when the application involves small amounts of mass such as IT-SOFC applications. Nonetheless it should be pointed out that, although conventional TPR experiments are dependent on experimental setup conditions, results are compatible with those acquired with XANES technique and are obtained with a simple, cost-effective equipment.

3.4 Catalytic experiments

In situ XANES catalytic experiments were performed in order to study the oxidation state of cations present in the metallic and support phases of samples NiO/ZDC and CuO–NiO/ZDC in partial oxidation of methane reaction conditions without a previous treatment in reducing conditions. The main aim was to correlate their redox properties with catalytic activity and compare their performance.

In Fig. 14a and b and the degree of Ce (α_{Ce}) and Ni (α_{Ni}) reduction are plotted against time altogether with the temperature profile for samples CuO–NiO/ZDC and NiO/ZDC respectively. Catalytic tests were performed altogether in a $CH_4 : O_2 = 2.6 : 1$ mol ratio feed flow as detailed in the experimental section, implying that methane is in stoichiometric excess for POM reaction. The results from reference spectra fitting corresponding to XANES Ce L3-edge measurements show that both samples exhibit a low degree of Ce reduction (<4%) in the whole temperature range. It is evident that α_{Ce} profiles differ from sample CuO–NiO/ZDC to sample NiO/ZDC. The degree of reduction increases stepwise in the whole temperature range for the latter sample while in the case of CuO–NiO/ZDC α_{Ce} slightly decreases when temperature is increased to 600 °C and again when temperature is increased to 700 °C. Taking into consideration the Ni K-edge results, it is evident that α_{Ni} increases stepwise with temperature in the whole temperature range for both samples. However, Ni reduction onset temperature is 50 °C lower for sample NiO/ZDC compared to sample CuO–NiO/ZDC.

In Fig. 15 and Table 2 the results of catalytic experiments in a conventional laboratory fixed bed reactor, previously reported, are presented. CuO–NiO/ZDC sample exhibits activity toward TOM at temperatures higher than 550 °C with *ca.* 100% CO_2 Selectivity at 600 °C and 650 °C.[14] Furthermore, when temperature is increased to 700 °C POM begins to take place with the consequent production of H_2 and CO. On the other hand, sample NiO/ZDC only exhibited activity towards POM after the

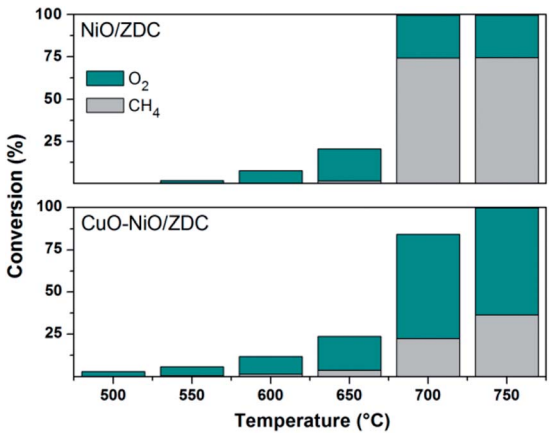

Fig. 15 Oxygen and methane conversion during catalytic experiments in conventional fixed bed reactor (conversion of x = $[(F_x^{in} - F_x^{out})/F_x^{in}]$, with F_x the molar flux of x) CuO–NiO/ZDC.

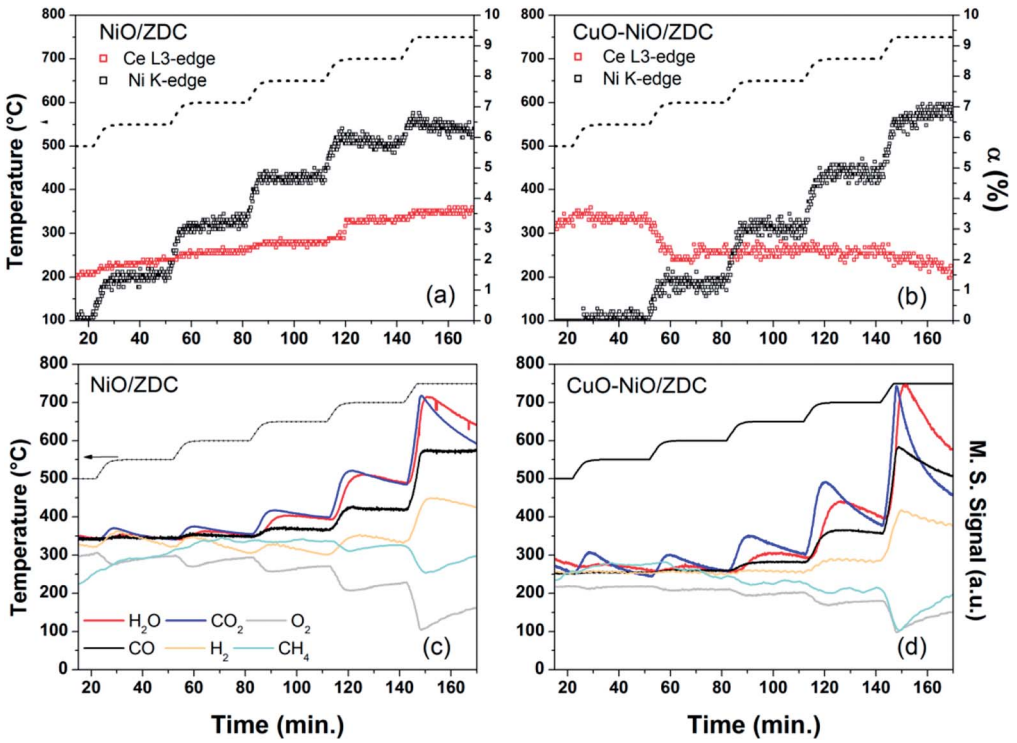

Fig. 14 (a) and (b) Degree of Ce reduction [$\alpha = Ce^{3+}/(Ce^{4+} + Ce^{3+})$], Ni reduction [$\alpha = Ni^0/(Ni^{2+} + Ni^0)$] and temperature *vs.* time during *in situ* XANES activity measurements for POM for samples NiO/ZDC and CuO–NiO/ZDC respectively. (c) and (d) Mass spectrometry data collected during *in situ* XANES experiments for POM activity for samples NiO/ZDC and CuO–NiO/ZDC respectively.

Table 2 Product distribution during catalytic experiments for POM in a conventional fixed bed reactor[a]

	CuO–NiO/ZDC				NiO/ZDC			
Temp. (°C)	SCO_2 (%)	SCO (%)	SH_2 (%)	RH_2 : CO	SCO_2 (%)	SCO (%)	SH_2 (%)	RH_2 : CO
600	100	0	0	0	0	0	0	0
650	97	0	0	0	0	0	0	0
700	40	60	34	1.2	2	97	100	2.2
750	23	77	55	1.5	1	99	100	2.2

[a] $SCO_x = FCO_x^{out}/(FCH_4^{in} - FCH_4^{out})$, $SH_2 = 0.5.\ FH_2^{out}/(FCH_4^{in} - FCH_4^{out})$, $RH_2 : CO = FH_2/FCO$, with F_x the molar flux of x.

light-off temperature of 700 °C was achieved, mainly detecting CO and H_2 and only traces of CO_2 as reaction products.

In line with this, it is interesting to correlate the XANES results in both Ce L3 and Ni K-edges with catalytic activity tests in fixed bed reactor: in the first place, between 500–550 °C CuO–NiO/ZDC sample exhibits a greater degree of Ce reduction when compared to the monometallic sample and is followed by a slight re-oxidation when increasing the temperature to 600 °C. At this same time Ni reduction is triggered for the bimetallic sample. This is a clear evidence of the interplay that exists between the redox behavior of both cations and the catalyst performance, being these redox changes strongly related to the activation of the sample toward TOM reaction. The fact that the ZDC present in CuO–NiO/ZDC sample is releasing oxygen from its lattice as a consequence of ceria reduction, might explain the delay in the reduction of the supported Ni^{2+}. In this sense, when NiO reduction begins, part of the oxygen released might be captured by the Ce present in the material to partially re-oxidize itself. Not to mention that TOM products are detected at this stage which are oxidizing in its nature. Furthermore, it should be mentioned that when temperature is raised to 700 °C Ce begins to re-oxidize while Ni continues its reduction tendency.

Secondly, taking into consideration NiO/ZDC sample, when POM is activated in fixed bed reactor experiments at 700 °C, Ce and Ni reduction is slightly promoted, being the steps proportionally larger that the previous ones. This larger reduction extent might be related to a more reducing environment caused by the formation of POM products (CO and H_2) and also possibly due to the H_2 generated by methane cracking ($CH_4 \rightarrow C + 2H_2$), one of the reactions related to carbon formation. In a previous work, carbonaceous residues were detected by XPD and SEM images of powders recovered after catalytic experiments with sample NiO/ZDC.[14] These results, altogether with a continuous reduction of Ce^{4+} to Ce^{3+} might imply that, although this sample is able to provide oxygen from its lattice, the rate at which carbon is oxidized is not fast enough to prevent carbon deposition. Furthermore, in sample NiO/ZDC after each temperature increase the degree of Ni reduction is increased as well. However, when there is a temperature dwell at temperatures above 650 °C there is a continuous re-oxidation of the sample, evidenced in the negative slope in the plot of α_{Ni} *vs.* time. It is noteworthy as well that the most pronounced Ce reduction step (*ca.* $\Delta\alpha_{Ce} = 1\%$) was registered when temperature was increased from 650 °C to 700 °C. This means that oxygen incoming either from the CeO_2–ZrO_2 lattice through Ce reduction or gas-phase oxygen are participating in the re-oxidation of Ni, a process strongly related to the catalyst deactivation.[40] On the contrary, in sample CuO–NiO/ZDC, Ni continues its reduction process while Ce begins to re-oxidize. It should be mentioned that no carbon formation was detected by XPD or SEM in the bimetallic sample. In Fig. 16 XPD patterns of spent catalysts are plotted. The presence of a Cu–Ni alloy in sample CuO–NiO/ZDC is evidenced altogether with the formation of graphitic carbon in sample NiO/ZDC.

Catalyst deactivation in Ni-based catalysts is mainly caused by carbon deposition, particle sintering and metalic site oxidation.[40] In our case, particle sintering was not a source of catalyst deactivation as samples were previously fired at 1000 °C and the maximum reaction temperature tested was 750 °C. In fact, a slight re-dispersion was found to take place due to sample reduction. Carbon formation was evidenced in monometallic NiO/ZDC sample both in SEM images with the presence of carbon filaments and in XPD patterns.[14] This was not the case of sample CuO–NiO/ZDC in which carbon formation was suppressed. However, an interesting finding in this work is that NiO/ZDC catalyst exhibits re-oxidation of active sites at 700 °C and 750 °C, temperatures at which sample was found to be active for POM and methane cracking. In the case of CuO–NiO/ZDC no re-oxidation takes place. Crozier *et al.* studied by means of *in situ* environmental TEM partial oxidation of methane reaction over Ni/SiO_2 catalysts.[41] They found that even after a pre-reduction of the sample, when heated up to 700 °C a re-oxidation took place due to the high O_2 partial pressures in

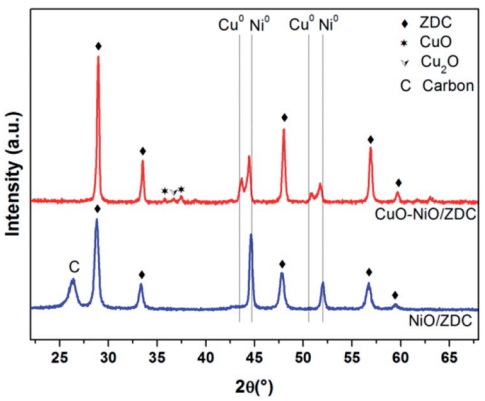

Fig. 16 XPD patterns of spent catalysts after conventional laboratory experiments.

the reactor. It should be noticed that they used a CH_4 : O_2 ratio of 8 : 4, which corresponds to the POM stoichiometry. They attribute this behavior to the high chemisorption energy of O_2 on Ni surface compared to CH_4, which favors a major O surface occupancy enhancing the kinetics of NiO formation. Therefore, as metallic Ni is the active site for POM to take place, NiO formation can cause Ni deactivation due to the loss of active sites for the reaction. Kitla *et al.* studied bimetallic copper/nickel catalysts supported on zirconia and ceria/zirconia for methane decomposition and reported that upon the addition of Cu to the supported Ni samples, the surface area of exposed Ni is significantly reduced.[42] They attributed this to the fact that upon reducing atmospheres a surface Cu-enriched CuNi alloy is formed. This process breaks up larger Ni ensembles that are supposed to be responsible for carbon formation. In addition, they reinforced the fact that the formation of this Cu-rich alloy modifies the properties of Ni, reducing the C–H bond breaking.

Mass spectrometry data collected during *in situ* XANES experiments for POM activity are plotted in Fig. 14c and d. In it, both catalysts exhibit CO_2 production above 550 °C. In particular, a peak of CO_2 and H_2O production is observed each time temperature is increased. This might be an indication that the reaction mechanism pathway for methane decomposition is the one that involves first TOM, followed by both steam and CO_2 methane reforming.[43] In conventional laboratory tests only small traces of CO_2 were detected with gas chromatography sampling for sample NiO/ZDC, while for sample CuO–NiO/ZDC activity towards total oxidation of methane was observed in the temperature range of 550 °C to 750 °C. In Fig. 14, CO production is evident above 600 °C for both samples while H_2 production is only observable above 650 °C for sample NiO/ZDC and above 700 °C for sample CuO–NiO/ZDC. The fact that H_2 is detected at higher temperatures than CO might indicate that H_2 is participating in Ni reduction. Methane signal does not fluctuate appreciably until 700 °C, indicating an important uptake only at 750 °C due to the fact that this reactant is present in stoichiometric excess. However, O_2 consumption is significant above 700 °C. Although in both cases a decrease in conversion for both reactants is observed, this might be related to the fact that a steady state has not been achieved in the 30 min temperature dwell. In fact, as analyzed above, the metallic phase in CuO–NiO/ZDC sample continues to reduce whilst the metallic phase in NiO/ZDC begins to re-oxidize.

4. Conclusions

In this work we analyzed by *in situ* XANES spectroscopy the effect of adding CuO to NiO/ZDC in terms of sample reducibility and catalytic activity. Results showed that the presence of Cu and/or Ni enhance Ce reduction, being this effect more pronounced for Cu-containing samples in the temperature range 650–800 °C. Ni reduction in all samples was found to take place in more than one step indicating that there are different Ni species present in the samples, each with different redox capabilities. CuO addition to the NiO/ZDC sample shifted the reduction profile to lower temperatures and also strongly influenced the shape and extent of the second step of reduction usually ascribed to the reduction of species strongly interacting with the support. Reduction onset temperature was found to depend on Ni crystallite size, being markedly promoted when samples exhibited low values of crystallite size.

In situ catalytic experiments for partial oxidation of methane showed a clear interplay between the redox behavior from the Ce in the CeO_2–ZrO_2 support and the Ni from the active phase. Ce reduction values remained low (<4%) during the experiments in the whole temperature range for both samples. However, clear behavior differences were detected in the Ce reduction profiles that shed light into the importance of the interaction of the support and the active phase in catalytic stability. At 750 °C a continuous reduction of Ce^{4+} to Ce^{3+} in sample NiO/ZDC and carbon formation detected in XPD patterns indicate that, although this sample is able to provide oxygen from its lattice, the rate at which carbon is oxidized is not fast enough to prevent carbon deposition. Furthermore, incoming oxygen either from the CeO_2–ZrO_2 lattice through Ce reduction or from gas-phase feed was found to favor re-oxidation of Ni at this temperature, a process strongly related to the catalyst deactivation. On the contrary sample CuO–NiO/ZDC exhibited a slight re-oxidation of Ce at 750 °C and no re-oxidation of Ni altogether with a clear suppression of carbon formation. These results were in agreement with those obtained through conventional catalytic tests performed in fixed-bed reactor, indicating that CuO addition to the NiO/ZDC system promotes stable catalytic activity and excellent resistance to formation of carbonaceous residues.

Conflicts of interest

The authors state that there are no conflicts of interest to declare.

Acknowledgements

The PhD scholarship granted by CONICET to Lucía M. Toscani is gratefully acknowledged. This work was supported by the National Synchrotron Light Laboratory (LNLS) under proposal XAFS1-15329 and received financial support from ANPCyT-PICT 2013 No. 1587.

References

1 S. P. S. Shaikh, A. Muchtar and M. R. Somalu, A review on the selection of anode materials for solid-oxide fuel cells, *Renewable Sustainable Energy Rev.*, 2015, **51**, 1–8.
2 C. Chatzichristodoulou, P. T. Blennow, M. Søgaard, P. V. Hendriksen and M. B. Mogensen, in *Catalysis by ceria and related materials*, ed. A. Trovarelli, Imperial College Press, London, 2013, vol. 12, pp. 623–783.
3 R. Di Monte and J. Kaspar, Nanostructured CeO_2-ZrO_2 mixed oxides, *J. Mater. Chem.*, 2005, **15**, 633–648.
4 M. G. Zimicz, S. A. Larrondo, R. J. Prado and D. G. Lamas, Time resolved in situ XANES study of the redox properties of $Ce_{0.9}Zr_{0.1}O_2$ mixed oxides, *Int. J. Hydrogen Energy*, 2012, **37**, 14881–14886.

5 M. G. Zimicz, D. G. Lamas and S. A. Larrondo, $Ce_{0.9}Zr_{0.1}O_2$ Nanocatalyst, influence of synthesis conditions in the reducibility and catalytic activity, *Catal. Commun.*, 2011, **15**, 68–73.

6 S. Pengpanich, V. Meeyoo and T. Rirksomboon, Catalytic oxidation of methane over CeO_2–ZrO_2 mixed oxide solid solution catalysts prepared via urea hydrolysis, *Appl. Catal., A*, 2002, **234**, 221–233.

7 S. A. Larrondo, A. Kodjaian, I. Fábregas, M. G. Zimicz, D. G. Lamas, N. E. Walsoe de Reca and N. E. Amadeo, Methane partial oxidation using $Ni/Ce_{0.9}Zr_{0.1}O_2$ catalysts, *Int. J. Hydrogen Energy*, 2008, **33**, 3607–3613.

8 M. G. Zimicz, F. D. Prado, D. G. Lamas and S. A. Larrondo, In situ XANES and XPD studies of $NiO/Ce_{0.9}Zr_{0.1}O_2$ IT-SOFCs anode nanomaterial as catalyst in the CPOM reaction, *Appl. Catal., A*, 2017, **542**, 296–305.

9 M. G. Zimicz, P. Núñez, J. C. Ruiz-Morales, D. G. Lamas and S. A. Larrondo, Electro-catalytic performance of 60%NiO/$Ce_{0.9}Zr_{0.1}O_2$ cermets as anodes of intermediate temperature solid Oxide fuel cells, *J. Power Sources*, 2013, **238**, 87–94.

10 S. Song, M. Han, J. Zhang and H. Fan, $NiCu\text{-}Zr_{0.1}Ce_{0.9}O_{2-d}$ anode materials for intermediate temperature solid oxide fuel cells using hydrocarbon fuels, *J. Power Sources*, 2013, **233**, 62–68.

11 S. Helveg, J. Sehested and J. R. Rostrup-Nielsen, Whisker carbon in perspective, *Catal. Today*, 2011, **178**, 42–46.

12 S. De, J. Zhang, R. Luque and N. Yan, Ni-based bimetallic heterogeneous catalysts for energy and environmental applications, *Energy Environ. Sci.*, 2016, **9**, 3314–3347.

13 H. Kim, C. Lu, W. L. Worrell, J. M. Vohs and R. J. Gorte, Cu-Ni Cermet anodes for direct oxidation of methane in solid-oxide fuel cells, *J. Electrochem. Soc.*, 2002, **149**, 247–250.

14 L. M. Toscani, M. G. Zimicz, J. R. Casanova and S. A. Larrondo, $Ni\text{-}Cu/Ce_{0.9}Zr_{0.1}O_2$ bimetallic cermets for electrochemical and catalytic applications, *Int. J. Hydrogen Energy*, 2014, **39**, 8759–8766.

15 L. De Rogatis, T. Montini, A. Cognini, L. Olivi and P. Fornasiero, Methane partial oxidation on NiCu-based catalysts, *Catal. Today*, 2009, **145**, 176–185.

16 A. Hornés, M. J. Escudero, L. Daza and A. Martínez-Arias, Electrochemical performance of a solid oxide fuel cell with an anode based on $Cu\text{-}Ni/CeO_2$ for methane oxidation, *J. Power Sources*, 2014, **249**, 520–526.

17 Z. Wang, W. Weng, K. Cheng, P. Du, G. Shen and G. Han, Catalytic modification of Ni-Sm-doped ceria anodes with copper for direct utilization of dry methane in low-temperature solid oxide fuel cells, *J. Power Sources*, 2008, **179**, 541–546.

18 A. Hornés, P. Bera, M. Fernández-García, A. Guerrero-Ruiz and A. Martínez-Arias, Catalytic and redox properties of bimetallic Cu-Ni systems combined with CeO_2 or Gd-doped CeO_2 for methane oxidation and decomposition, *Appl. Catal., B*, 2012, **111–112**, 96–105.

19 L. P. Matte, A. S. Kilian, L. Luza, M. C. M. Alves, J. Morais, D. L. Baptista, J. Dupont and F. Bernardi, Influence of the CeO_2 support on the reduction properties of Cu/CeO_2 and Ni/CeO_2 nanoparticles, *J. Phys. Chem. C*, 2015, **119**, 26459–26470.

20 A. Jha, D. W. Jeong, W. J. Jang, C. V. Rode and H. S. Roh, Mesoporous $NiCu\text{-}CeO_2$ oxide catalysts for high-temperature water-gas shift reaction, *RSC Adv.*, 2015, **5**, 1430–1437.

21 M. G. Zimicz, I. O. Fábregas, D. G. Lamas and S. A. Larrondo, Effect of synthesis conditions on the nanopowder properties of $Ce_{0.9}Zr_{0.1}O_2$, *Mater. Res. Bull.*, 2011, **46**, 850–857.

22 B. Ravel and M. Newville, ATHENA, ARTEMIS, HEPHAESTUS: Data Analysis for X-ray Absorption Spectroscopy using IFEFFIT, *J. Synchrotron Radiat.*, 2005, **12**, 537–554.

23 V. M. González-DelaCruz, J. P. Holgado, R. Pereñíguez and A. Caballero, Morphology changes induced by strong metal-support interaction on a Ni-ceriacatalytic system, *J. Catal.*, 2008, **257**, 307–314.

24 P. Fornasiero, G. Balducci, R. Di Monte, J. Kaspar, V. Sergo, G. Gubitosa, A. Ferrero and M. Graziani, Modification of the redox behaviour of CeO_2 induced by structural doping with ZrO_2, *J. Catal.*, 1996, **164**, 173–183.

25 L. J. Kundakovic and M. Flytziani-Stephanopoulos, Reduction characteristics of copper oxide in cerium and zirconium oxide systems, *Appl. Catal., A*, 1998, **171**, 13–29.

26 T. A. Maia and E. M. Assaf, Catalytic features of Ni supported on CeO_2-ZrO_2 solid solution in the steam reforming of glycerol for syngas production, *RSC Adv.*, 2014, **4**, 31142–31154.

27 E. Moretti, L. Storaro, A. Talon, P. Riello, A. Infantes Molina and E. Rodríguez-Castellón, 3-D flower like Ce–Zr–Cu mixed oxide systems in the CO preferential oxidation (CO-PROX): Effect of catalyst composition, *Appl. Catal., B*, 2015, **168–169**, 3855.

28 V. Sharma, P. A. Crozier, R. Sharma and J. B. Adams, Direct observation of hydrogen spillover in Ni-loaded Pr-doped ceria, *Catal. Today*, 2012, **180**, 2–8.

29 X. Tang, B. Zhang, Y. Li, Y. Xu, Q. Xin and W. Shen, Carbon monoxide oxidation over CuO/CeO_2 catalysts, *Catal. Today*, 2004, **93–95**, 191–198.

30 A. R. Nagash, T. H. Etsell and S. Xu, XRD and XPS Study of Cu-Ni Interactions on Reduced Copper-Nickel-Aluminum Oxide Solid Solution Catalysts, *Chem. Mater.*, 2006, **18**, 2480–2488.

31 H. S. Roh, K. W. Jun, W. S. Dong, J. S. Chang, S. E. Park and Y. I. Joe, Highly active and stable $Ni/Ce\text{-}ZrO_2$ catalyst for H_2 production from methane, *J. Mol. Catal. A: Chem.*, 2002, **181**, 137–142.

32 Y. Shen and A. C. Lua, Sol-gel synthesis of Ni and Ni supported catalysts for hydrogen production by methane decomposition, *RSC Adv.*, 2014, **4**, 42159–42167.

33 P. Li, J. Liu, N. Nag and P. A. Crozier, In situ preparation of $Ni\text{-}Cu/TiO_2$, *J. Catal.*, 2009, **262**, 73–82.

34 N. J. Divins, I. Angurell, C. Escudero, V. Pérez-Dieste and J. Llorca, Influence of the support on surface rearrangements of bimetallic nanoparticles in real catalysts, *Science*, 2014, **346**, 620–623.

35 S. Bernal, J. J. Calvino, M. A. Cauqui, J. M. Gatica, C. López Cartes, J. A. Pérez Omil and J. M. Pintado, Some contributions of electron microscopy to the characterization of the strong metal-support interaction effect, *Catal. Today*, 2003, **77**, 385–406.

36 A. I. Frenkel, S. Khalid, J. C. Hanson and M. Nachtegaal, in *In-situ Characterization of Heterogeneous Catalysts*, ed. J. A. Rodriguez, J. C. Hanson and P. J. Chupas, John Wiley & Sons, 2013, vol. 1, pp. 23–47.

37 G. Silversmit, H. Poelman, V. Balcaen, P. M. Heynderickx, M. Olea, S. Nikitenko, W. Bras, P. F. Smet, D. Poelman, R. De Gryse, M. F. Reniers and G. B. Marin, In-situ XAS on the Cu and Ce local structural changes in a CuO-CeO_2 catalyst under propane reduction and re-oxidation, *J. Phys. Chem. Solids*, 2009, **70**, 1274–1284.

38 G. R. Rao, S. K. Meher, B. G. Mishra and P. H. K. Charan, Nature and catalytic activity of bimetallic CuNi particles on CeO_2 support, *Catal. Today*, 2012, **198**, 140–147.

39 P. Malet and A. Caballero, The selection of experimental conditions in temperature-programmed reduction experiments, *J. Chem. Soc., Faraday Trans. 1*, 1988, **84**, 2369–2375.

40 E. Ruckenstein and H. Y. Wang, Carbon deposition and catalytic deactivation during CO_2 reforming of CH_4 over Co/γ-Al_2O_3 catalysts, *J. Catal.*, 2002, **205**, 289–293.

41 S. Chenna, R. Banerjee and P. A. Crozier, Atomic-scale observation of the Ni activation process for partial oxidation of methane using in situ environmental TEM, *ChemCatChem*, 2011, **3**, 1051–1059.

42 A. Kitla, O. V. Safonova and K. Fottinger, Infrared studies on bimetallic copper/nickel catalysts supported on zirconia and ceria/zirconia, *Catal. Lett.*, 2013, **143**, 517–530.

43 T. Shishido, M. Sukenobu, H. Morioka, M. Kondo, Y. Wang, K. Takaki and K. Takehira, Partial oxidation of methane over Ni/Mg-Al oxide catalysts prepared by solid phase crystallization method from Mg-Al hydrotalcite-like precursors, *Appl. Catal., A*, 2002, **223**, 35–42.